Spin-orbit coupling effect on the thermopower and power factor of CoSbS

Raveena Gupta [1,2] and Chandan Bera [1,*]

[1]*Institute of Nano Science and Technology, Habitat Center, Phase-X, Mohali, Punjab 160062, India*
[2]*Centre for Nanoscience and Nanotechnology, Panjab University, Sector-25, Chandigarh 160036, India*

A recent experimental paper by Du *et al.* [Phys. Rev. Lett. **123**, 076602 (2019)] had shown colossal values of thermopower at 40 K. The Seebeck coefficient values decrease with the application of magnetic field. We found that the colossal Seebeck coefficient is due to carrier correlation and large increase in effective mass. The reduction of thermopower with magnetic field is explained by including spin-orbit interaction terms in our calculations. By tuning atomistic magnetic moment, the power factor of thermoelectric materials can be further optimized. We have shown that a 10^7 times increase in power factor is possible by increasing magnetic field.

I. INTRODUCTION

Thermoelectric materials play a key role in reducing environmental pollution by converting heat energy to electrical energy and are attractive for renewable power generation [1,2]. Efficiency of a thermoelectric material is given by a dimensionless quantity known as the figure of merit (ZT), which is defined as $ZT = \frac{S^2 \sigma T}{\kappa}$, where S is the Seebeck coefficient, σ is the electrical conductivity, κ is the total thermal conductivity, and T is the absolute temperature. Thus a good thermoelectric material must have higher electrical conductivity and low thermal conductivity. Though at temperatures above 500 K, higher figure of merit has been achieved in third generation thermoelectrics [3,4], efficiencies in the temperature range 5–250 K are still relatively poor. Thermoelectricity is also needed below room temperature for the thermoelectric cooling mechanism which is used in next-generation refrigerating technologies. At such temperatures, for high figure of merit, the thermoelectric power factor must be large. Chalcogenides of cobalt (Co) have been identified as promising materials for thermoelectric applications due to their high Seebeck coefficient and high electrical conductivity [5–7]. Out of all chalcogenides of cobalt, CoSbS has been seen to show ZT values of 0.40 at 800 K [8]. Moreover, higher ZT values have also been reported for optimized CoSbS based materials [9]. A recent work by Du *et al.* [10] reporting high thermopower value at 40 K encouraged this theoretical work.

Herein, we report the effect of including spin-orbit interaction terms on the thermoelectric power factor of CoSbS by using Boltzmann transport equations. This work shows the origin of high thermopower at low temperature and also the reason for the reduction in Seebeck coefficient values with magnetic field. A further high power factor can be achieved by tuning the atomistic magnetic moment with the applied magnetic field at cryogenic temperatures.

II. THEORETICAL METHODS

The electronic properties of CoSbS were investigated by density functional theory (DFT) simulations using the Vienna *ab initio* simulation package (VASP) [11] based on the projector augmented wave method (PAW) [12,13] with a plane-wave basis set and periodic boundary conditions. The exchange correlation energy was calculated using the Perdew-Burke-Ernzerhof (PBE) functional [14]. The cutoff energy for the plane wave basis was set to 350 eV with an energy convergence threshold of 10^{-8} eV. All the atoms were relaxed until the forces on them were less than 0.001 eV/Å. The lattice structure of CoSbS belongs to the *Pbca* space group with lattice parameters $a = 5.833$ Å, $b = 5.966$ Å, and $c = 11.691$ Å obtained after relaxation. Spin-orbit coupling (SOC), which is an effect that couples the orbital and spin degrees of freedom in the system, was also included in the simulations via an **L·S** term, where **L** is the angular momentum and **S** is the spin. The inclusion of the spin-orbit coupling term adds an additional term $H_{SOC} \propto \vec{\sigma} \cdot \vec{L}$ to the Hamiltonian that couples Pauli spin operator $\vec{\sigma}$ with angular momentum operator $\vec{L}$. As a relativistic correction, SOC acts predominantly in the immediate vicinity of the nuclei, such that it is assumed that contributions of H_{SOC} outside the PAW spheres are negligible. In VASP, SOC is calculated via nonlinear magnetism terms and it only works for PAW potentials. Magnetic moments of $0.0\mu_B$, $0.1\mu_B$, $0.2\mu_B$, and $0.5\mu_B$ were given for the cobalt atoms using noncollinear SOC calculations. The electronic band structures along a path connecting characteristic points in the Brillouin zone with the inclusion of SOC for different magnetic moments are shown in Fig. 1.

The electrical transport properties were calculated in a temperature range of 5 K to 400 K using the Boltzmann transport equations as implemented in BoltzTraP2 [15] using the constant relaxation time approach and also by including the temperature dependent relaxation time due to electron-phonon scattering.
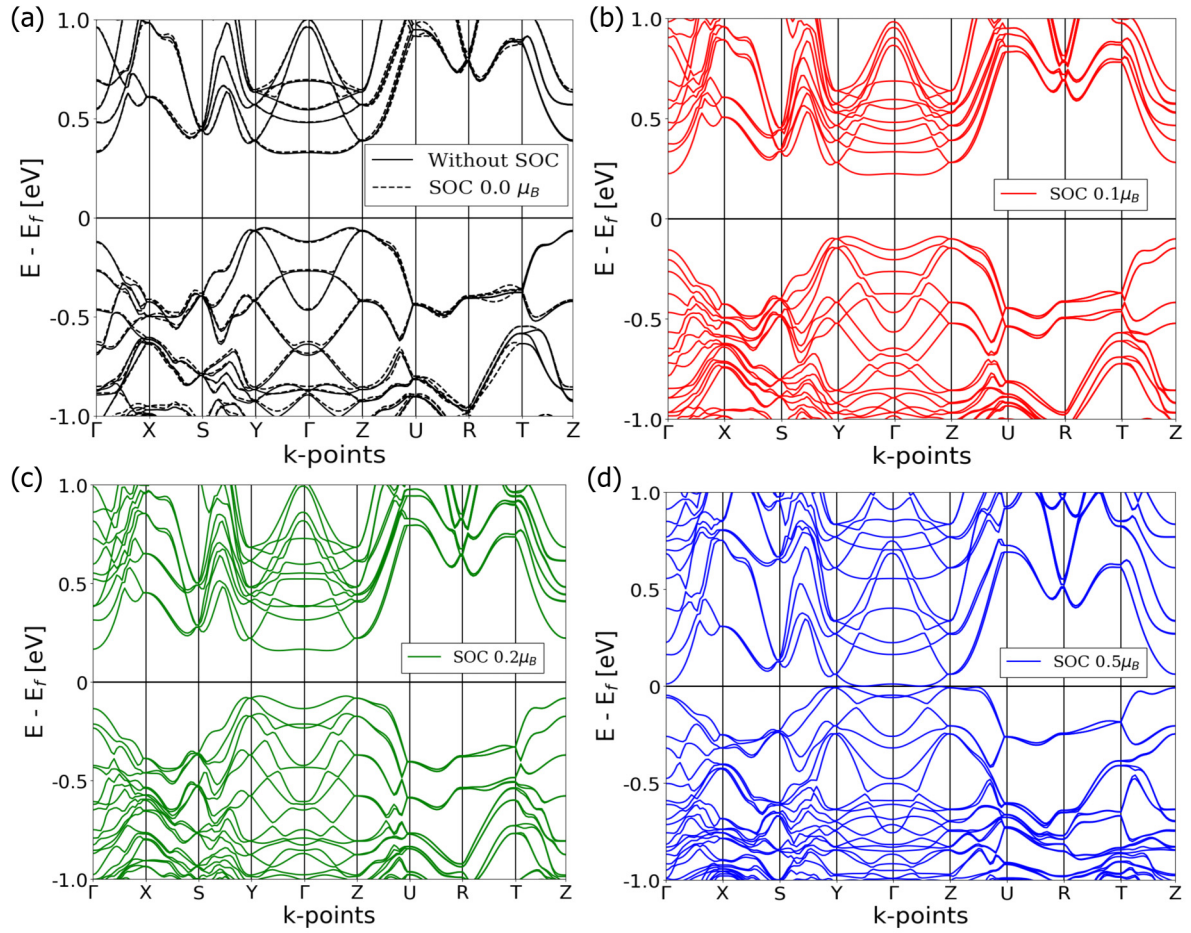
―――――
*chandan@inst.ac.in

FIG. 1. Electronic band structure of CoSbS (a) without SOC and atomistic magnetic moment $0.0\mu_B$ and (b) with atomistic magnetic moment $0.1\mu_B$ (c) $0.2\mu_B$, and (d) $0.5\mu_B$.

In the relaxation time approximation, the thermoelectric coefficients are expressed as [15]

$$\sigma = e^2 \int_{-\infty}^{\infty} d\epsilon \left(-\frac{\partial f_0}{\partial \varepsilon} \right) \Sigma(\epsilon, T), \tag{1}$$

$$S = \frac{e}{T\sigma} \int_{-\infty}^{\infty} d\epsilon \left(-\frac{\partial f_0}{\partial \varepsilon} \right) \Sigma(\epsilon, T)(\epsilon - \mu), \tag{2}$$

$$\kappa_{\text{el}} = \frac{1}{T} \int_{-\infty}^{\infty} d\epsilon \left(-\frac{\partial f_0}{\partial \varepsilon} \right) \Sigma(\epsilon, T)(\epsilon - \mu)^2 - \sigma S^2 T. \tag{3}$$

In the above equations, $\Sigma(\epsilon, T)$ is the transport distribution function, which can be obtained by summing over electron bands (b) and integrating over the Brillouin zone as $\Sigma(\epsilon, T) = \int \frac{d^3\mathbf{k}}{8\pi^3} \sum_b v_{b,\mathbf{k}}^2 \tau_{b,\mathbf{k}} \delta(\epsilon - \epsilon_{b,\mathbf{k}})$, $v(\epsilon)$ is the component of the group velocity of each carrier in the transport direction, $\epsilon_{b,\mathbf{k}}$ is the energy of that electronic state, $\tau_{b,\mathbf{k}}$ is its total relaxation time, e is the electronic charge, T is the temperature, and μ is the chemical potential.

The electron-phonon scattering rate is given by [16]

$$\frac{1}{\tau_{e-ph}} = \frac{k_B T_L \pi N(\epsilon) E_D^2}{u_s^2 \rho \hbar}, \tag{4}$$

where k_B is the Boltzmann constant, T_L is the lattice temperature, ρ is the density of the medium ($6.93\,\text{g cm}^{-3}$), u_s is the velocity of sound in the medium ($4292\,\text{ms}^{-1}$), and E_D is the deformation potential which is taken to be 38 eV as calculated by Lie *et al.* [6].

The effective mass as a function of temperature is calculated using [17]

$$n(T, \mu) = \frac{1}{2\pi} \left(\frac{2m^*(T, \mu)k_B T}{\hbar^2} \right)^{3/2} F_{1/2}(\eta_{\text{eff}}), \tag{5}$$

where $n(T, \mu)$ is the carrier concentration, T is the temperature, and η_{eff} is the effective reduced chemical potential calculated from the Seebeck coefficient given by [18]

$$S(T, \mu) = \frac{k_B}{e} \left[\frac{(2 + \lambda)[F_{1+\lambda}(\eta_{\text{eff}})]}{(1 + \lambda)[F_\lambda(\eta_{\text{eff}})]} - \eta_{\text{eff}} \right], \tag{6}$$

where λ is the scattering exponent whose value is set to 1/2. $F_{1+\lambda}$ are the Fermi functions given by

$$F_j(\eta) = \int_0^{\infty} \frac{e^j d\epsilon}{1 + e^{\epsilon - \eta}}. \tag{7}$$

The force calculations were done in the $2 \times 2 \times 1$ supercell using a $2 \times 2 \times 1$ k-point mesh. Displacements with an amplitude of 0.01 Å are used for calculating forces with VASP in order to obtain interatomic force constants. Frozen phonon approach is adopted for extracting the force constants as implemented in the program PHONOPY [19]. Spin-orbit coupling (SOC) was included via an **L·S** term and magnetic moments of $0.0\mu_B$, $0.2\mu_B$, and $0.5\mu_B$ were given for the cobalt atoms. Figure 2 shows the phonon band structures thus obtained for CoSbS without SOC and by including SOC with magnetic moments.

III. RESULTS AND DISCUSSION

As shown in Fig. 1(a), the valence band has flatter regions at Γ point, which are responsible for higher Seebeck coefficient of the compound at low temperature due to the descent of holes from valence band maxima (VBM) to Γ point. The strength of the spin-orbit coupling shows up indirectly in the calculated quantities as the magnetic moments are varied. SOC influences band-edge energies by splitting the atomic orbital energy. As we increase the magnetic moments ($\mu_B > 0$), the strength of the spin-orbit coupling increases which leads to splitting of the band energies and shifting of valence band maxima (VBM) towards conduction band minima (CBM) along Γ-Y and Γ-Z directions. This shifting of VBM towards CBM leads to reduction in energy band gap with increasing magnetic moment. CoSbS has a band gap of 0.33 eV, which reduces to 0.22 eV on application of $0.1\mu_B$ magnetic moment. Magnetic moment of $0.5\mu_B$ decreases the band gap to 0.0 eV.

Temperature dependant electrical conductivity (σ) and Seebeck coefficient (S) by using the electron phonon scattering rate given by Eq. (4) are shown in Figs. 3(a) and 3(b), respectively. Seebeck coefficient shows a peak at 1.86 mV/K at 40 K as compared to the experimentally reported [10] value of 2.5 mV/K at the same temperature. This peak consistently appears at 40 K for the atomic magnetic moments $0.1\mu_B$ and $0.2\mu_B$ and a slight shift is observed for $0.5\mu_B$ moment at Co position. Though in experimental investigation by Du *et al.* [10], CoSbS was found paramagnetic, a high magnetic field induced a magnetic moment in Co atom. This atomistic magnetic moment induces a strong spin-orbit coupling which has a significant contribution on the thermoelectric properties of CoSbS. At the temperature 40 K, for atomistic magnetic moment $\mu_B = 0.5$, there is less than two times reduction in the Seebeck coefficient and a 10^8 times enhancement is observed in the electrical conductivity value. Thus our relaxation time model based on deformation potentials and band energies gives results closer to experimental values. We did not observe large change in carrier concentration and electron relaxation time with temperature and μ_B [Figs. 4(a) and 4(b)]. At 300 K, the carrier concentration is of the order of $\sim 10^{18}$ cm^{-3} and it decreased to $\sim 10^{13}$ cm^{-3} below 100 K.

At 40 K, effective mass shows an increment to 5.4 from free electron mass. This higher effective mass is a strong indication of carrier correlations and heavy valence band as indicated by Du *et al.* [10]. We also observe large variation of chemical potential (μ) with magnetic moment [Fig. 4(d)]. The
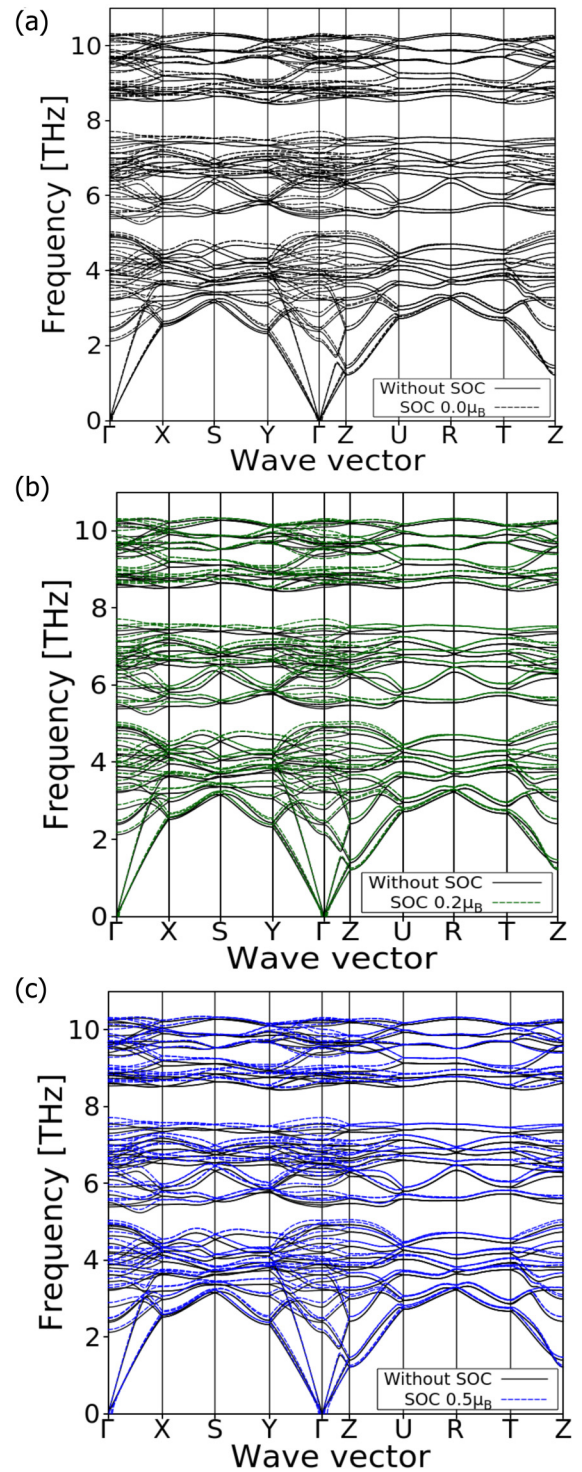

FIG. 2. Phonon band structure of CoSbS (a) without SOC and atomistic magnetic moment $0.0\mu_B$ and (b) with atomistic magnetic moment $0.2\mu_B$ and (c) $0.5\mu_B$.

chemical potential is very low for $\mu = 0.0\mu_B$ and it slowly increases with application of magnetic moment. The diffusion of holes from VBM (valence band maxima) to the lower valence band decreases with application of magnetic moments due to large energy splitting, which explains the reduction in the peak value of the Seebeck coefficient with magnetic
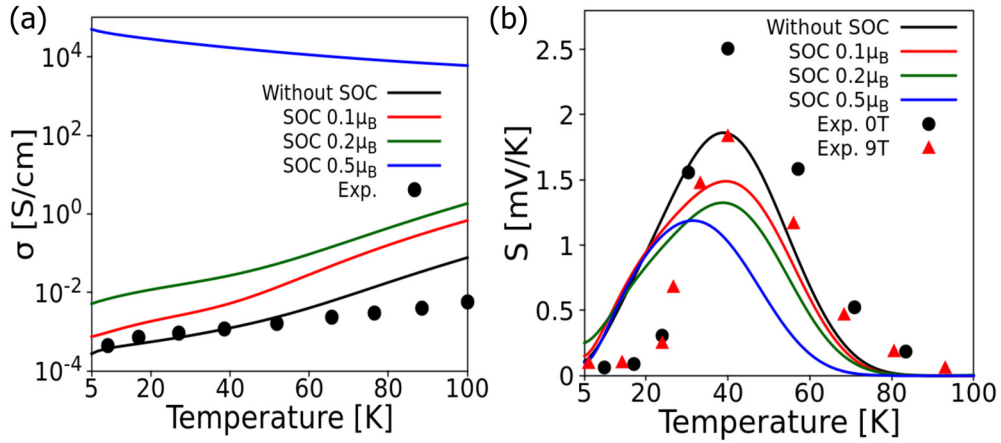
FIG. 3. Variation of (a) electrical conductivity and (b) Seebeck coefficient, with temperature for CoSbS (without SOC) and by applying magnetic moments $0.1\mu_B$, $0.2\mu_B$, and $0.5\mu_B$ along with experimental values [10] (the black circles represent experimental value corresponding to 0 T field and the red triangles represent experimental values corresponding to 9 T field) using electron-phonon scattering rate.

field [Fig. 3(b)] and change in effective mass of the carrier [Fig. 4(c)].

For magnetic moment $0.1\mu_B$, the Seebeck coefficient drops to 1.5 mV/K at 40 K, which further reduces to 1.2 mV/K for $0.5\mu_B$. A peak shift from 40 K to 30 K is seen for $0.5\mu_B$. When calculated without SOC and with small magnetic moments, the electrical conductivity [Fig. 3(a)] increases with temperature showing semiconducting behavior. For

magnetic moment $0.5\mu_B$, the effect of SOC is significant as the band gap reduces to 0.0 eV and the material starts showing metal-like properties, with conductivity decreasing with temperature.

The Seebeck coefficient is also calculated with a constant relaxation time (CRTA) as per BoltzTraP [18] as seen in Fig. 5. Energy and temperature independent relaxation time ($\tau = 10^{-15}$ s) is used for CRTA calculations. A very
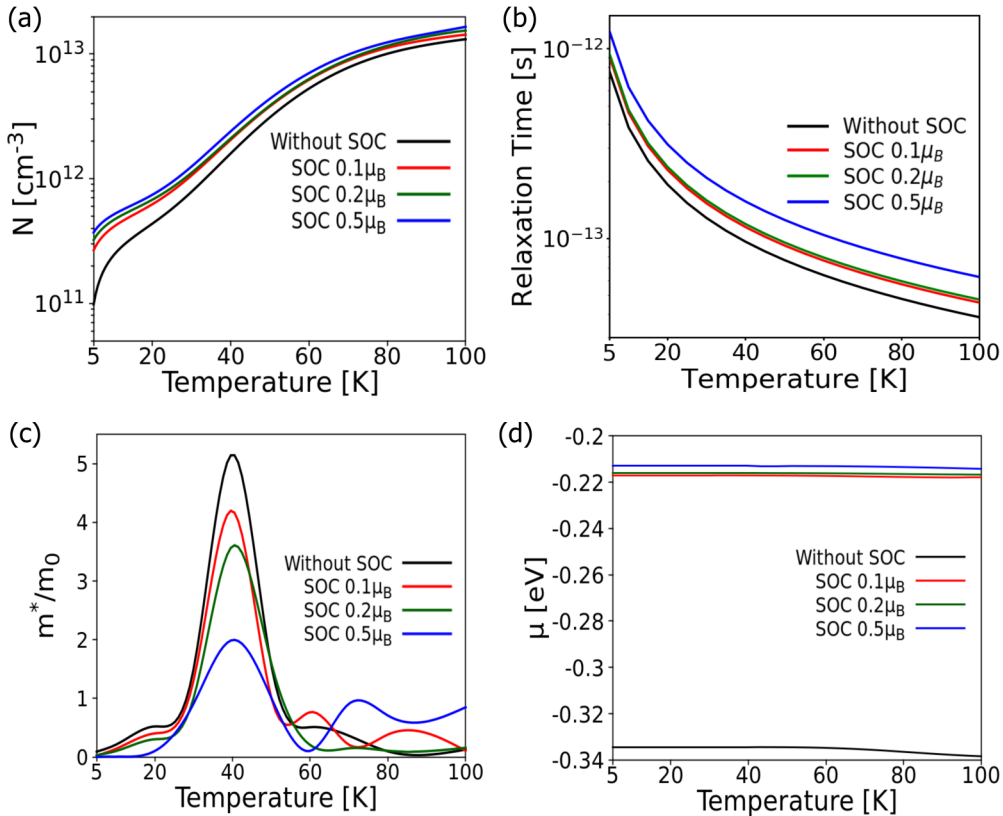

FIG. 4. Variation of (a) carrier concentration, (b) relaxation time, (c) effective mass, and (d) chemical potential, with temperature for CoSbS (without SOC) and by applying magnetic moments $0.1\mu_B$, $0.2\mu_B$, and $0.5\mu_B$.
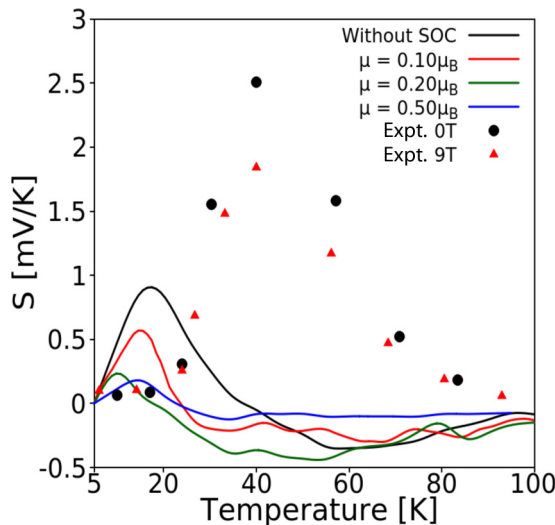
FIG. 5. Variation of Seebeck coefficient with temperature for CoSbS (without SOC) and by applying magnetic moments $0.1\mu_B$, $0.2\mu_B$, and $0.5\mu_B$ along with experimental values [10] (the black circles represent experimental value corresponding to 0 T field and the red triangles represent experimental values corresponding to 9 T field) for constant relaxation time.

significant contrast is observed in CRTA calculation. The Seebeck coefficient has a *p*-type to *n*-type transition at $T = 30$ K, whereas no such transition is observed in experiment and theoretical calculation with energy dependent relaxation time ($\tau_{e\text{-}ph}$). Hence our modeled relaxation time based on deformation potentials and band energies gives results closer to experimental values [10].

Figure 6 shows the variation of power factor ($S^2\sigma$) with temperature for two temperature ranges (5–100 K and 100–400 K). It is seen that the power factor when calculated without SOC and magnetic moments $0.1\mu_B$ and $0.2\mu_B$ increases with temperature.

At 5 K the power factor ($S^2\sigma$) is $3.18 \times 10^{-5} \mu$W cm^{-1}K^{-2} (Fig. 6), which increases to 55.31 μW cm^{-1}K^{-2} at 400 K without magnetic field or without SOC calculations. For magnetic moment $0.2\mu_B$, there is an increase in the power factor by about one order of magnitude compared to $0.1\mu_B$ or without the SOC case. At 5 K, for magnetic moment $0.5\mu_B$,
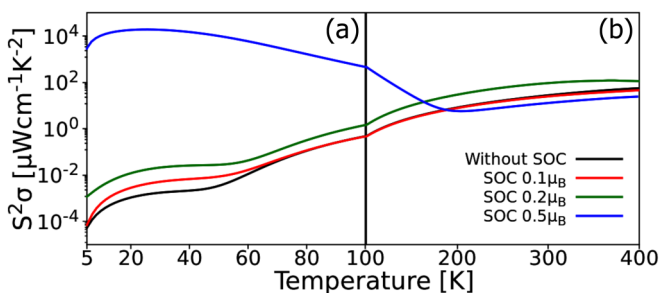

FIG. 6. Variation of power factor with temperature for temperature scales (a) 5 K to 100 K and (b) 100 K to 400 K, for CoSbS (without SOC) and by applying magnetic moments $0.1\mu_B$, $0.2\mu_B$, and $0.5\mu_B$.

the power factor is $4.97 \times 10^2 \mu$W cm^{-1}K^{-2}, which is $\sim 10^7$ times higher than that for without SOC and $\sim 10^5$ times higher than that for $0.2\mu_B$. However, beyond 100 K, the power factor starts to decrease rapidly and there is a crossover at around 200 K for $\mu_B = 0.5$. The power factor for $0.5\mu_B$ becomes 24.1 μW cm^{-1}K^{-2} at 400 K, much lower than that without SOC value. Hence, though the higher magnetic moment or field can increases the power factor at cryogenic temperatures, a magnetic moment of $0.2\mu_B$ is more useful above room temperature. This variation of power factor is directly related to the temperature dependence of the Seebeck coefficient and electrical conductivity with magnetic field.

As seen from phonon dispersion plots (Fig. 2), SOC has no significant effect on the phonon properties. At a very high magnetic moment $\mu = 0.5\mu_B$, almost no change in acoustic mode is observed. There is a very small shift in the optical mode. So there will be no effect of spin-orbit coupling on the lattice thermal conductivity, although there is a large effect on the power factor at lower temperatures.

IV. CONCLUSION

In conclusion, we report the theoretical calculation of low temperature electrical properties of CoSbS with the effect of including spin-orbit coupling terms on the electronic structure. Here, we show a high Seebeck coefficient at cryogenic temperatures which is in qualitative agreement with experimental values [10] with a peak of 1.86 mV/K at 40 K. The increase in Seebeck coefficient is explained in terms of carrier concentration and strong carrier correlations. The reduction of the Seebeck coefficient with magnetic field is due to the relativistic effect induced by atomistic magnetic moment in the structure. The electrical conductivity calculation with SOC and $0.5\mu_B$ atomistic magnetic moment on Co atoms shows a metal-like behavior due to a strong effect on inclusion of spin-orbit coupling terms and a larger shift of VBM towards CBM leading to closure of the energy band gap. The power factor calculations show that, though higher magnetic moment included by SOC ($0.5\mu_B$) gives a huge power factor of the order of $\sim 10^2 \mu$W cm^{-1}K^{-2} at cryogenic temperatures, it rapidly decreases above 100 K. Large enhancement in power factor may be possible in the cryogenic range by tuning the atomic moment of Co. Spin-orbit coupling with magnetic moment at the Co site has no effect on the phonon dispersion of CoSbS. Therefore, thermal properties will not be affected by the external magnetic field, although there is a large effect of it on the power factor at lower temperatures. This work calls for further investigation of electrical properties of CosbS by application of magnetic field.

[1] J. Yang and T. Caillat, Thermoelectric materials for space and automotive power generation, MRS Bull. **31**, 224 (2006).

[2] M. Zebarjadi, K. Esfarjani, M. S. Dresselhaus, Z. F. Ren, and G. Chen, Perspectives on thermoelectrics: from fundamentals to device applications, Energy Environ. Sci. **5**, 5147 (2012).

[3] L. D. Zhao, S. H. Lo, Y. Zhang, H. Sun, G. Tan, C. Uher, C. Wolverton, V. P. Dravid, and M. G. Kanatzidis, Ultralow thermal conductivity and high thermoelectric figure of merit in SnSe crystals, Nature (London) **508**, 373 (2014).

[4] K. Biswas, J. He, I. D. Blum, C. I. Wu, T. P. Hogan, D. N. Seidman, V. P. Dravid, and M. G. Kanatzidis, High-performance bulk thermoelectrics with all-scale hierarchical architectures, Nature (London) **489**, 414 (2012).

[5] D. Parker, A. F. May, H. Wang, M. A. McGuire, B. C. Sales, and D. J. Singh, Electronic and thermoelectric properties of CoSbS and FeSbS, Phys. Rev. B **88**, 159902(E) (2013).

[6] Z. Liu, H. Geng, J. Shuai, Z. Wang, J. Mao, D. Wang, Q. Jie, W. Cai, J. Sui, and Z. Ren, The effect of nickel doping on electron and phonon transport in the n-type nanostructured thermoelectric material CoSbS, J. Mater. Chem. C **3**, 10442 (2015).

[7] R. Chmielowski, S. Bhattacharya, W. Xie, D. Péré, S. Jacob, R. Stern, K. Moriya, A. Weidenkaff, G. K. H. Madsen, and G. Dennler, High thermoelectric performance of tellurium doped paracostibite, J. Mater. Chem. C **4**, 3094 (2016).

[8] P. Kaur and C. Bera, Effect of alloying on thermal conductivity and thermoelectric properties of CoAsS and CoSbS, Phys. Chem. Chem. Phys. **19**, 24928 (2017).

[9] S. Bhattacharya and G. K. H. Madsen, A novel p-type half-Heusler from high-throughput transport and defect calculations, J. Mater. Chem. C **4**, 11261 (2016).

[10] Q. Du, M. Abeykoon, Y. Liu, G. Kotliar, and C. Petrovic, Low-Temperature Thermopower in CoSbS, Phys. Rev. Lett. **123**, 076602 (2019).

[11] G. Kresse and D. Joubert, From ultrasoft pseudopotentials to the projector augmented-wave method, Phys. Rev. B **59**, 1758 (1999).

[12] P. E. Blöchl, Projector augmented-wave method, Phys. Rev. B **50**, 17953 (1994).

[13] D. Vanderbilt, Soft self-consistent pseudopotentials in a generalized eigenvalue formalism, Phys. Rev. B **41**, 7892 (1990).

[14] J. P. Perdew, K. Burke, and M. Ernzerhof, Generalized Gradient Approximation Made Simple, Phys. Rev. Lett. **77**, 3865 (1996).

[15] G. K. H. Madsen, J. Carrete, and M. J. Verstraete, BoltzTraP2, a program for interpolating band structures and calculating semi-classical transport coefficients, Comput. Phys. Commun. **231**, 140 (2018).

[16] C. Bera, M. Soulier, C. Navone, G. Roux, J. Simon, S. Volz, and N. Mingo, Thermoelectric properties of nanostructured $Si_{1-x}Ge_x$ and potential for further improvement, J. Appl. Phys. **108**, 124306 (2010).

[17] Z. M. Gibbs, F. Ricci, G. Li, H. Zhu, K. Persson, G. Ceder, G. Hautier, A. Jain, and G. J. Snyder, Effective mass and fermi surface complexity factor from ab initio band structure calculations, npj Comput. Mater. **3**, 2057 (2017).

[18] G. K. H. Madsen and D. J. Singh, BoltzTraP. a code for calculating band-structure dependent quantities, Comput. Phys. Commun. **175**, 67 (2006).

[19] A. Togo, F. Oba, and I. Tanaka, First-principles calculations of the ferroelastic transition between rutile-type and $CaCl_2$-type SiO_2 at high pressures, Phys. Rev. B **78**, 134106 (2008).